The University of Nottingham
UNITED KINGDOM · CHINA · MALAYSIA

Salih, Omar S. and Ou, Hengan and Sun, W. and McCartney, D.G. (2015) A review of friction stir welding of aluminium matrix composites. Materials & Design, 86 . pp. 61-71. ISSN 0264-1275

Access from the University of Nottingham repository:
http://eprints.nottingham.ac.uk/42956/1/Review%20of%20FSW%20of%20AMC_MD_2015.pdf

Copyright and reuse:

The Nottingham ePrints service makes this work by researchers of the University of Nottingham available open access under the following conditions.

This article is made available under the Creative Commons Attribution licence and may be reused according to the conditions of the licence. For more details see: http://creativecommons.org/licenses/by/2.5/

A note on versions:

The version presented here may differ from the published version or from the version of record. If you wish to cite this item you are advised to consult the publisher's version. Please see the repository url above for details on accessing the published version and note that access may require a subscription.

For more information, please contact eprints@nottingham.ac.uk

Materials and Design 86 (2015) 61–71

Contents lists available at ScienceDirect

Materials and Design

journal homepage: www.elsevier.com/locate/jmad

A review of friction stir welding of aluminium matrix composites

Omar S. Salih *, Hengan Ou *, W. Sun, D.G. McCartney

Department of Mechanical, Materials and Manufacturing Engineering, Faculty of Engineering, The University of Nottingham, Nottingham NG7 2RD, UK

ARTICLE INFO

Article history:
Received 7 June 2015
Received in revised form 10 July 2015
Accepted 12 July 2015
Available online 20 July 2015

Keywords:
Friction stir welding
Aluminium matrix composites
Macrostructure and microstructure
Mechanical properties
Tool wear

ABSTRACT

As a solid state joining process, friction stir welding (FSW) has proven to be a promising approach for joining aluminium matrix composites (AMCs). However, challenges still remain in using FSW to join AMCs even with considerable progress having been made in recent years. This review paper provides an overview of the state-of-the-art of FSW of AMC materials. Specific attention and critical assessment have been given to: (a) the macrostructure and microstructure of AMC joints, (b) the evaluation of mechanical properties of joints, and (c) the wear of FSW tools due to the presence of reinforcement materials in aluminium matrices. This review concludes with recommendations for future research directions.

© 2015 The Authors. Published by Elsevier Ltd. This is an open access article under the CC BY license (http://creativecommons.org/licenses/by/4.0/).

1. Introduction

Advanced materials like aluminium matrix composites (AMCs) have attracted considerable attention due to their appealing mechanical properties and a clear potential for aerospace applications. They are thus viewed as an ideal candidate as a new generation of light weight and high strength materials [1–3]. However, the implementation of AMCs is restricted and they are not widely used in the aviation industry, in part because of the difficulties that are related to the joining of these metals by conventional welding processes [2,4].

Efficient joints in terms of strength of AMC materials cannot be achieved by fusion based welding methods due to the reaction between reinforcements and matrices leading to the formation of brittle secondary phases in the weld pool or decomposition of reinforcements in molten metal [4,5]. With respect to welding processes, it has been proven by several studies that more efficient joints with much reduced porosity, cracking, distortion, and reinforcement dissolution can be achieved when friction stir welding (FSW) is adopted. However, as a result of the presence of reinforcement particles, a major difficulty of welding AMCs by FSW is the narrow welding window (the range of welding parameters by which successful welding can be accomplished without defects) in comparison with a monolithic aluminium alloy.

In recent years, several review papers have been published on various aspects of FSW. Thomas et al. [6], Rai et al. [7], and Zhang et al. [8] comprehensively reviewed FSW tools and development. Threadgill et al. [9] gave a critical overview of FSW of aluminium alloys. Mishra and Ma [10] gave a systematic review on FSW and friction stir processing (FSP). Tutum and Hattel [11] reviewed the numerical optimisation of FSW and its challenges and Çam [12] provided a comprehensive overview of FSW development for different metals and alloys.

However, there is little information related to FSW of AMCs. The present review paper firstly gives a brief description on the FSW process, metal matrix composites (MMCs), and the weldability of aluminium alloys and AMCs in Sections 2 to 4. This is followed by a detailed evaluation of a number of critical issues in FSW of similar AMCs focusing on the macrostructure and microstructure, mechanical properties of AMC joints, as well as tool wear in Sections 5 to 7. Finally, conclusions are drawn with a particular view on future challenges and research directions.

2. Brief review of FSW

The invention of the FSW process in 1991 was made by The Welding Institute (TWI) in the United Kingdom as a solid state joining process for joining aluminium alloys [13]. The peak welding temperature can be limited to 80% of the melting temperature of the base metal (BM). Therefore, this process can be considered as a hot working process. As FSW has been widely used to join aluminium alloys, it may be developed as a viable route to join AMCs especially for high strength non-weldable series (AA2xxx, AA6xxx, and AA7xxx), which are susceptible to solidification cracking in the weld zone and liquation cracking in

Abbreviations: AMC, aluminium matrix composite; AS, advancing side; BM, base metal; EBW, electron beam welding; FSP, friction stir processing; FSW, friction stir welding; GTA, gas tungsten arc; HAZ, heat affected zone; HSS, high speed steel; LBW, laser beam welding; MMC, metal matrix composite; NZ, nugget zone; PWHT, post-weld heat treatment; RS, retreating side; TMAZ, thermo-mechanically affected zone; UTS, ultimate tensile strength.

* Corresponding authors.
E-mail addresses: epxosa@nottingham.ac.uk (O.S. Salih), h.ou@nottingham.ac.uk (H. Ou).

http://dx.doi.org/10.1016/j.matdes.2015.07.071
0264-1275/© 2015 The Authors. Published by Elsevier Ltd. This is an open access article under the CC BY license (http://creativecommons.org/licenses/by/4.0/).

the heat affected zone (HAZ) [14]. Dissimilar joints of AMCs or with different metals can be manufactured by using FSW without concerns for composition compatibility, which is an important consideration in fusion welding to avoid solidification cracking [10].

FSW is an ideal process for producing low cost and high performance joints. The practical approach of FSW is to use a non-consumable rotating tool consisting of two parts including a shoulder and a pin. During FSW the pin is inserted into the faying surface of the plates and then moved horizontally in the direction of the joint line as shown in Fig. 1. The surface of the tool has dual actions for heat generation and mechanical sweeping of softened metal. The heat input through the frictional action between the tool and workpiece leads to softening of the area around the pin. Meanwhile, the softened materials are swept in the form of severe plastic deformation from the advancing side (AS) to the retreating side (RS) to form a solid state joint. The advancing and retreating sides of the plates to be joined are defined by the direction of tool rotation (clockwise or anti-clockwise) and the traverse movement of the tool. Plate side is defined as advancing if the tool movement is in the same direction of the tool rotation, whilst it is retreating if the tool moves in the opposite direction (see Fig. 1). Different types of joint like butt, lap, and T-joints can be welded successfully by FSW [8,10,15].

Moreover, FSW is considered as a green and environmentally friendly welding technology because of low energy consumption, no gas emission, and no need for consumable material such as electrodes, filler metals, and shielding gases (normally present in fusion welding processes). A survey carried out by the American Welding Society (AWS) in 2002 showed that $34.4 billion per year is spent on arc welding including the use of consumables, repair, and energy consumption in the USA. The adoption of FSW has increased rapidly and 10% of joining processes have reportedly been replaced by FSW [16].

3. Brief overview of MMCs

In recent years, MMCs have attracted considerable attention for critical applications in industrial sectors such as spacecraft structures, deck panels, and automotive and railway brake discs. The global demand for MMCs is expected to increase from about 5496 tons to nearly 8000 tons in the period from 2012 to 2019, and it is continuously rising as shown in Fig. 2 [17].

Light metals like aluminium, magnesium, and titanium alloys are considered as ideal base matrices to produce MMCs reinforced by carbide, nitride, boride, and oxide in the form of particles, whiskers, and fibres [18] as shown in Fig. 3 [19]. MMCs can possess unique properties including good thermal conductivity, low coefficient of thermal expansion, low specific density, high specific stiffness, good dimensional stability, and excellent strength to weight ratio depending on the type of reinforcements used [20–22]. As a result of these desirable properties, MMCs have been used to withstand excessive space environmental

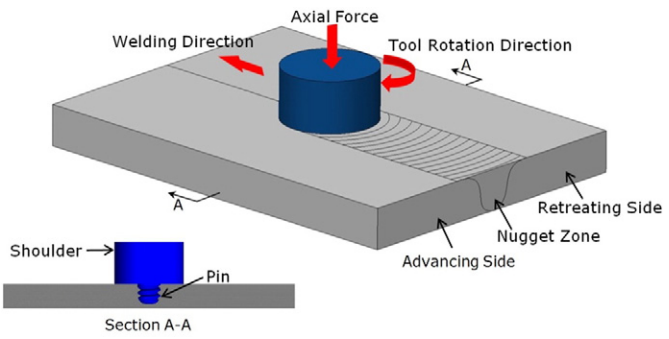

Fig. 1. Schematic drawing of FSW.

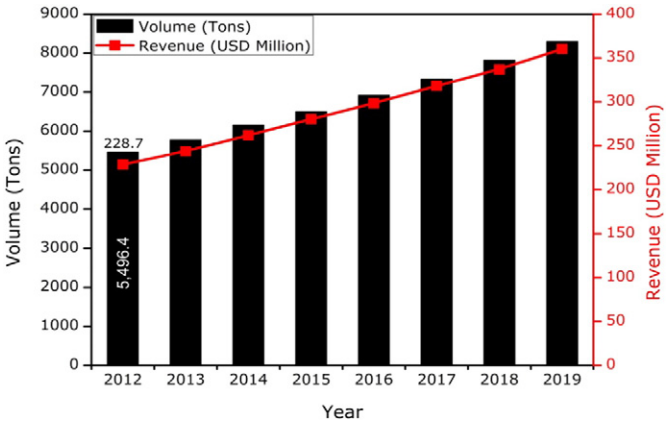

Fig. 2. Global demand for MMCs [17].

condition of substantial changes in temperature. For example, the International Space Station is exposed to varying temperatures from +125 °C to −125 °C as it orbits around the earth [23].

As a versatile material, AMCs may be selected as an alternative to high strength aluminium alloys in aeroengines and aerospace structures like fins, wings, and fuselage. In 2001 NASA used composite aluminium Al–Li 2195 rather than aluminium alloy Al 2219 for the external fuel tank of space shuttles leading to a reduction of weight by 3400 kg. This saving in weight increases the cargo capacity of space shuttles and enables it to transport more than one components in a single flight to the International Space Station [24]. Also, the use B/Al in truss and frame of aeroplanes saved 45% weight from an all aluminium design. Another application of AMCs is a 3.6 m antenna for Hubble Space Telescope manufactured from Gr/Al (P100/6061 Al). It offers high stiffness, superb electrical conductivity, and low coefficient of thermal expansion [23]. In addition, AMCs have found a wide range of applications in military sector such as armour, due to the combined static strength and high ballistic performance [10].

4. Weldability of aluminium alloys and AMCs

The strength of pure aluminium is inadequate for structural applications. Therefore, to eliminate this limitation it is alloyed with other metals like copper, manganese, magnesium, zinc, and silicon. Different mechanical properties can be achieved by controlling the amount of alloying elements and heat treatments. Aluminium and its alloys are often considered as formable and ductile due to their face-centred cubic crystal structure and are available in wrought and cast forms. The former can be produced, typically, by semi-continuous direct chill casting followed by rolling (hot or cold), extrusion, and forging, whilst the latter can be made from sand casting, lost wax casting, permanent steel mould casting, and die-casting. Wrought aluminium is classified into two types depending on the main alloying elements. Non heat treatable weldable aluminium alloys including AA1xxx, AA3xxx, and AA5xxx series are strengthened by cold working, whereas AA2xxx, AA6xxx and AA7xxx series are heat treatable, non-weldable alloys that can be strengthened by precipitation hardening [25,26].

In general, welding of aluminium and its alloys needs considerable attention. Problems may occur including the loss of strength and defect formation when fusion welding processes are used. Trapped porosity may also appear in the cross section, due to the dissolution of shielding gases (oxygen, nitrogen and hydrogen) or moisture in the electrode and flux in molten metal as shown in Fig. 4. Furthermore, lack of fusion occurs in part due to the high melting temperature up to 2060 °C of stable aluminium oxide on the surface. Centre-line or solidification cracking is also a serious problem in fusion welding of aluminium alloys as shown in Fig. 5. This failure occurs as a result of stresses induced by metal

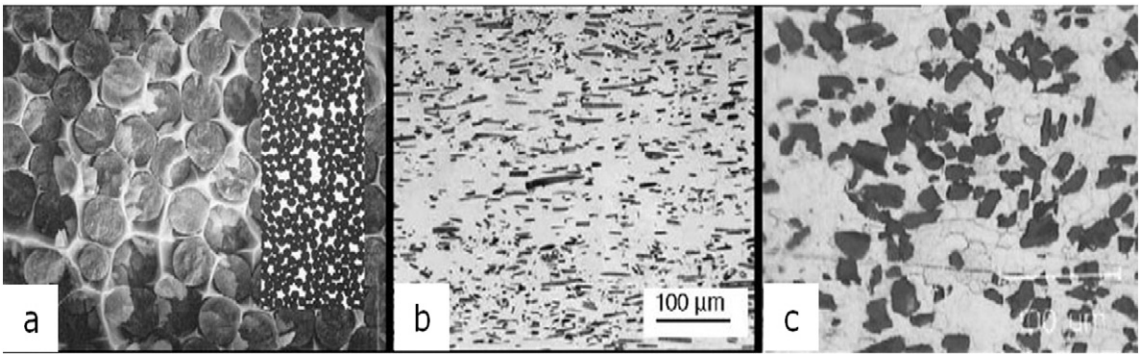

Fig. 3. Reinforcement types — (a) fibres, (b) whiskers, and (c) particles [19].

contraction in cooling and the often large difference between the liquidus temperature and eutectic or final solidification temperature. The variations in heating and cooling cycle in the HAZ normally result in lowered the strength of joint in heat treatable alloys [25,27].

In addition to the aforementioned problems accompanied by welding of aluminium and its alloys, other difficulties come into view when AMCs are welded by fusion welding processes including: (a) incomplete mixing between filler and BM, (b) the formation of excess eutectic, (c) the presence of large size porosity of more than 100 μm in the fusion zone, and (d) reaction between molten metals and reinforcements resulting in undesirable phases such as Al_4C_3 [10]. A study was reported by Storjohann et al. [28] to compare three types of fusion welding (GTA, LBW, and EBW) with heat inputs of 165, 108, and 5.9 J/mm, respectively, with solid state welding (FSW) to fabricate similar AMC joints for AA6061/Al_2O_3/20p (20% volume of Al_2O_3 particles) and AA2124/SiC/20w (20% Volume of SiC whiskers). They found that in all fusion welding processes Al_2O_3 particles completely dissolved in molten aluminium leading to the reduction in the strength of joints as shown in Fig. 6. In the case of SiC whiskers, the formation of Al_4C_3 and precipitation of a Si-rich phase occurred as a result of fast reaction between the reinforcement and molten metal as shown in Fig. 7. In contrast, a good joint was achieved by FSW and there was no significant change in reinforcement volume fraction for both AMC joints. Therefore, the findings of this study gave a clear indication of the suitability of FSW to weld different types of AMCs.

5. Macrostructure and microstructure of FSW joints in AMCs

The quality of a weld joint can be assessed primarily by the evaluation of macrostructure and microstructure. The workpieces are exposed to thermal cycles and severe plastic deformation at high temperature through the rotation of the tool in FSW. As a result of either excessive or insufficient heat input in the weld zone, defects such as tunnel defects and kissing bonds may occur in the welded joint. Also there are significant changes in the shape and structure of the welding zone. Hence suitable welding parameters need to be selected to avoid these defects. Therefore, the evaluation of macrostructure and microstructure of FSW joints has been carried out extensively.

5.1. Macrostructure of AMC joints

The macrostructure examination of welding zone can be used to reveal the quality of welded joints. Four different zones; weld or nugget zone (NZ), thermo-mechanically affected zone (TMAZ), HAZ and BM can be identified in the macrostructure of AMC joints as shown in Fig. 8. Wake effect, shape of the NZ, onion ring structure, and tunnel defect are typical features which can be examined visually or at low magnification. Several conditions like types of BM, workpiece thickness, welding parameters, and shape of tool play a significant role in the formation of these features.

The first feature is characterised by the so called wake effect at the surface of plates. Both Kalaiselvan et al. [30] and Ceschini et al. [31] reported that the formation of the wake effect by FSW of AA6061/B_4C and AA7005/Al_2O_3/10p plates, respectively. They considered that it was the friction action between the tool shoulder and the horizontal movement on the surface of the plate that led to the formation of wake effect during FSW.

The shape of NZ is the second feature which can be identified by macrostructural examination. Mishra and Ma [10] classified the shape of NZ into two profiles, basin and elliptical as shown in Fig. 9. Feng et al. [32] reported the formation of elliptical shape of the NZ in AA2009/SiC/15p weldment at 600 rpm. They also noticed that the post-weld heat treatment (PWHT) did not affect the profile of the NZ. Recently, Ni et al. [29] and Wang et al. [33] reported that the basin shaped NZ was obtained by FSW using the same material (AA2009/SiC/15p) at higher rotation speeds at 800 and 1000 rpm, respectively, which gives an indication about the effect of tool rotation speed on the NZ shape.

The third feature that characterises the NZ is the appearance of onion ring structure in swirl pattern as shown in Fig. 10. Cavaliere et al. [34] and Ceschini et al. [35] mentioned that the formation of the onion ring structure through the cross section weld of AA6061/Al_2O_3/20p plates. They considered that the flow behaviour of softened metals and the differences in dislocation density during the joining process are the main reasons for the formation of the onion ring structure. Bozkurt et al. [36] reported that the sweeping of softened metals and the horizontal movement of the FSW tool are the key mechanism for the formation of the onion ring structure when joining AA2124/SiC/25p. Nami

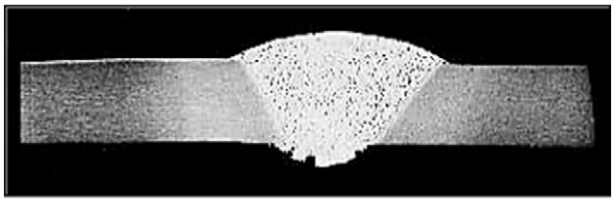

Fig. 4. Trapped porosity in a fusion weld [25].

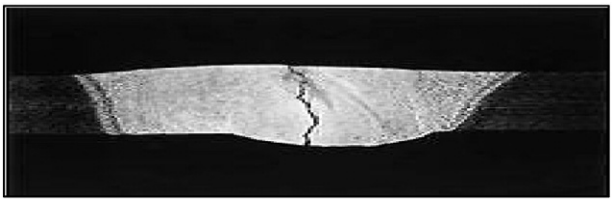

Fig. 5. Centre-line cracks in AA6082 plate/4043 filler metal TIG weld [25].

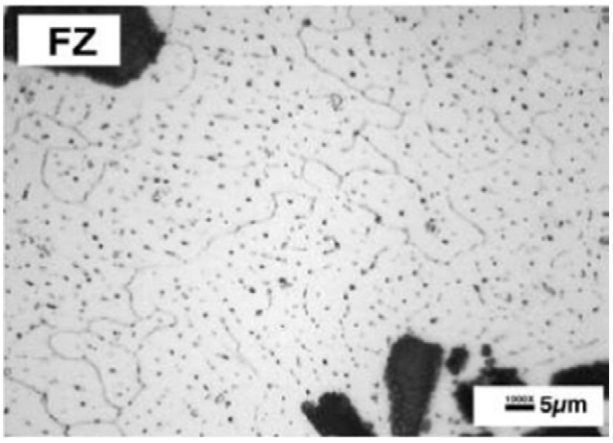

Fig. 6. Optical micrograph of a laser beam fusion weld in AA6061/Al_2O_3/20p [28].

et al. [37] explained that the formation of onion ring structure in FSW Al/Mg_2Si/15p depends on the effect of grain geometry and difference in grain size. They clarified that an alternating layer of Mg_2Si eutectic needle and fine particle Mg_2Si was found in rich and small bands, respectively. Also they pointed out that the number of FSW passes can change the distribution and volume of Mg_2Si in the NZ.

However, onion ring structure can partially appear or disappear completely under certain conditions due to the type of AMCs, recrystallization characteristics, and plate thickness. Chen et al. [38] and Marzoli et al. [39] found that the formation of the onion ring was not visible in the AS but clearly visible in the RS in FSW AA6063/B_4C-T5 and 6061/Al_2O_3/20p, respectively, as shown in Fig. 11. This was attributed to the partial recrystallization which happened in the weld zone and hindered the flow of metal by reinforcement. Furthermore, Ni et al. [29] and Wang et al. [33] reported that there was no visible onion ring in a basin shaped weld zone in FSW AA2009/SiC/17p-T351 and AA2009/SiC/15p-T4, respectively. They reckoned that the reduction in thickness led to the disappearance of the onion rings.

Fig. 12 shows the tunnel defect that can be identified by macrostructure examination. It is found that the frequency of tunnel defect generation in FSW depends on the speed of tool rotation. The appearance of this type of defect can be attributed to insufficient heat input or inappropriate flow of plasticized metal. Cioffi et al. [40] identified clearly the appearance of tunnel defect in the AS of FSW AA2124/SiC/25p at a low rotation speed of 300 rpm. The tunnel defect is less likely to happen as the rotation speed increases to 800 rpm which produces defect free joints. They claimed that higher speed allowed higher energy input and hence sufficient plastic flow for minimised tunnel defects. Similarly,

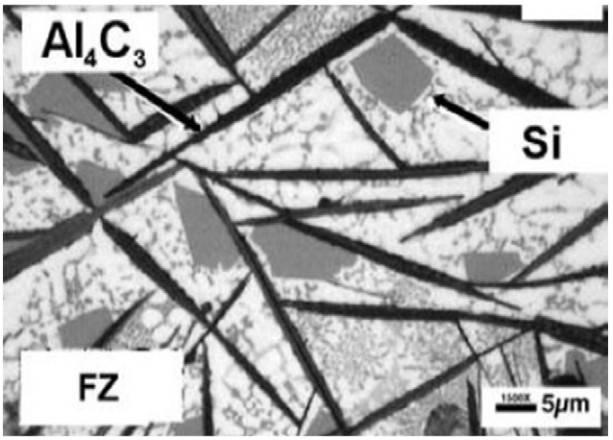

Fig. 7. Optical micrograph of a laser beam fusion weld in AA2124/SiC/20w [28].

Fig. 8. Cross-sectional macrostructure of FSW AA2009/SiC/17p joint [29].

Nami et al. [37] reported tunnel defect in FSW Al/Mg_2Si/15p at low and high rotation speeds. They argued that tunnel defect occurred due to improper flowability of metal in the stir zone as results of either lack of heat input at low rotation speeds between 710 and 900 rpm or excessive heat at higher rotation speeds between 1300 and 1400 rpm.

Periyasamy et al. [42] studied the effect of heat input on the metallurgical properties of a AA6061/SiC/10p joint. The evaluation was carried out at five heat inputs of 755, 850, 945, 1039, and 1133 J/mm obtained by applying five tool rotation speeds through calculation. They found that the metal flows intermittently if heat input was below 1039 J/mm, whilst turbulent flow behaviour occurred at a higher value of more than 1039 J/mm. Tunnel defect appeared in the AS of the fabricated joint at heat input of 1133 J/mm as a result of excessive flow of plasticized metal to the upper surface. Interestingly, this observation was confirmed recently by Fu et al. [43] when studying FSW of high strength aluminium alloy AA7050. They indicated that the submerged FSW (plate under water by 3 cm) gave high quality joint (tunnel defect free) than that welded in air. In addition, the location of tunnel defect in FSW in air can occur either in the bottom or on the top region of the AS.

In conclusion, wake effect, nugget shape, onion ring, and tunnel defect are the main macrostructure features of AMCs welded by FSW. Rotation speed and amount of heat input have a great effect on the nugget shape and tunnel defects, whilst material flow behaviour, recrystallization, and plate thickness effect are main factors for the appearance of onion ring. Hence the quality of AMC joints can be improved if the temperature of the weld zone can be carefully controlled.

5.2. Microstructure of AMC joints

The heat generated through the rotation of FSW tool ideally reaches approximately 0.8 of the melting temperature of the joined AMCs. This leads to reinforcement redistribution and refinement, recrystallization, and grain growth in the NZ. The microstructure of the AMC shows that the reinforcement materials are clustered and distributed heterogeneously in the matrix as a result of production processes (casting or powder metallurgy). The inhomogeneous distributions of reinforcement materials in the microstructure of the BM can affect the isotropy of mechanical properties. It is accepted that the stirring action during FSW causes a break up of clustered reinforcement and homogenous distribution in the weld zone due to the mixing of material and severe plastic deformation [29,30,36,37,40,44]. In contrast, Periyasamy et al. [42] reported that the NZ of AA6061/SiC/10p joints fabricated at a heat input below 1039 J/mm consisted of coarsely clustered SiC particles.

Meanwhile, the size of Al_2O_3 and SiC particles decreases obviously as compared to the original material and the particle edges can be rounded or blunted in the NZ. As a result, the aspect ratio of the particles decreases noticeably. This phenomenon may be explained by the abrasion and stirring effect between particles and tool pin circumference, shoulder surface during welding process [28,29,39,45]. Ceschini et al. [35] pointed out that finer particles were formed closer to the shoulder of the tool than the tip of the pin. However, if the size of original reinforcement is small it is not exposed to the refinement process. For example, Storjohann et al. [28] reported that no change was noticed in the size of SiCw reinforcement with a diameter of 1–2 μm and length of 5–7 μm. Instead the whiskers were reoriented as shown in Fig. 13, whilst 20 μm Al_2O_3 particles were subjected to refinement during FSW.

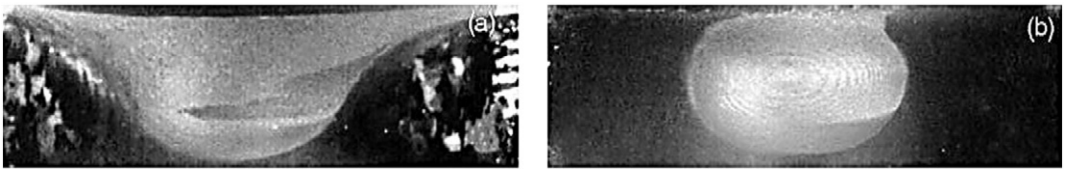

Fig. 9. Nugget shape — (a) basin, (b) elliptical [10].

The NZ may be characterised by equiaxed grains much smaller than those in the BM. This indicated that new grains nucleated in the NZ during FSW as a result of dynamic recrystallization. Feng et al. [32] reported that an obvious reduction in grain size of the NZ reached to about 5 μm in FSW of 8 mm thickness AA2009/SiC/15p plate. Grain growth occurs after PWHT to a T4 condition which leads to a grain size of 8 μm. Similar observations were made by Wang et al. [33]. They reported that the reduction of grain size from 10 μm to 6 μm taking place in the NZ of FSW 6 mm thick AA2009/SiC/15p plate. They believe that the high energy point on SiCp broken surface is the main location of the nucleation and growth of nano-size grains to decrease the aluminium matrix/reinforcement interface free energy. However, the growth of new grains in T4 PWHT was restricted by the presence of SiC particles. In addition, Periyasamy et al. [42] indicated that a fine grain structure, fine eutectic, and the elimination of dendritic structure in the NZ were achieved at high heat input through the increase of tool rotation speed. On the other hand, faster cooling rate due to low heat input leads to the formation of coarser grains because of incomplete recrystallization in the NZ of AA6061/SiC/10p FSW joint.

In summary, the evaluation of microstructure of AMCs welded by FSW showed an improvement in reinforcement distribution and refined particles due to the stirring action in FSW. Also the formation of new grains with equiaxed dimensions occurs as a result of dynamic recrystallization process.

6. Mechanical properties of FSW joints in AMCs

For FSW of AMC joints, the evaluation of mechanical properties including microhardness, tensile strength, and fatigue is of considerable importance particularly for critical components. It is also possible to optimise the welding parameters based on the evaluation of these properties which reflect the joint efficiency (the ratio of the tensile strength of joint to the tensile strength of base metal) of the weldment.

6.1. Microhardness of AMC joints

Transverse microhardness through the cross section of a welded joint can give an indication about the change of various phases and reinforcement distribution in FSW of AMCs. Two different profiles of microhardness curves have been observed in the joint cross section of AMC weldment.

Firstly, it is well accepted that the highest hardness value occurs in the centre of the NZ followed by a gradual decrease across the TMAZ and HAZ until reaching the hardness value of the BM as shown in Fig. 14 [30,32,34,37,42,45–48]. This is attributed to more grain refinement in the NZ due to dynamic recrystallization and more uniform distribution of finer reinforcement particles in the weld zone due to FSW action. These conclusions agreed with the Hall–Petch equation (inversely proportional relation between hardness and grain size) and the Orowan hardening mechanism (hardness can be improved if finer particles distribute homogenously) [47]. Also it may be concluded from Fig. 14 that lower heat input leads to the formation of coarse grains because of incomplete recrystallization and thus a reduction of the NZ microhardness.

Secondly, Fig. 15 shows the "W" shape profiles of microhardness curves which can be obtained in FSW of AMC joint, as reported by a number of researchers [29,36,40,49]. Bozkurt et al. [36] explained that the behaviour of this curve depended on the amount of induced dislocation and particle refinement for AA2124/SiC/25p–T4 FSW joint. The microhardness of the BM was nearly 185 Hv (Vickers hardness). Meanwhile the hardness of the NZ was 170 and 165 Hv in the root and top of the joint, respectively. The generation of dislocation due to the difference in thermal expansion between aluminium matrix and reinforcements particles was more significant in the NZ than in the HAZ. Therefore, the HAZ showed lower hardness on both the AS and the RS than that of the NZ, which was only about 155 Hv.

6.2. Tensile strength of AMC joints

The tensile strength of AMC joints fabricated by FSW was compared to that of the BM. The efficiency of joint produced by FSW is higher than that fabricated by conventional welding methods. Many factors influence the tensile strength of AMC joint including tool design, welding parameters, PWHT, and the formation of intermetallic compound. Table 1 summarises the tensile properties of AMCs welded by FSW.

6.2.1. Effect of tool design

The shape of tool shoulder and pin plays a significant role in the tensile strength of FSW joints. Vijay and Murugan [54] investigated the effect of different pin shapes (square, hexagonal, and octagon) in tapered and un-tapered profile on the tensile properties of FSW Al/TiB_2/10. The joint efficiency fabricated by un-tapered square pin exhibits a maximum tensile strength which reaches 99.47% of that of the BM in comparison to other profiles. This is attributed to the high ratios of static volume to dynamic volume of plasticized material, measured as 1.56 for square pin, 1.21 and 1.11 for hexagon and octagon profiles, respectively. This result was confirmed in a later study by Hassan et al. [55]. They used un-tapered (square, hexagonal, and octagon) pin profiles to join hybrid AMC (Al–4%Mg, 1% SiCp and 1% graphite particles). Wang et al. [49] found that the use of conical threaded pin at high traverse speed at 800 mm/min rather than a flat cylinder in joining AA2009/SiC/17p led to an increase of the joint efficiency to 97% due to the improvement of the flowability of softened material. In a study reported by Yigezu et al. [56] in FSW 5 mm thick Al–12%Si/TiC/10 plates, three

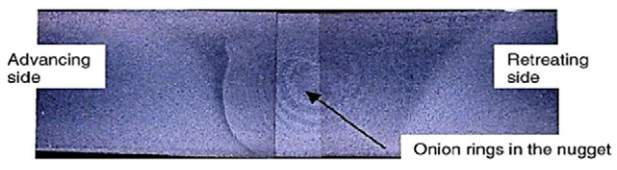

Fig. 10. Optical micrograph of an onion ring feature in FSW AA6061/Al_2O_3/20p cross-section [35].

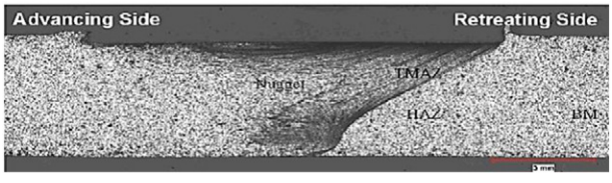

Fig. 11. Partial appearance of an onion ring in a cross-section of an AA6063/B_4C/10.5p welded by FSW [38].

Fig. 12. Tunnel defect in cross-section morphology of an AA6061/AlN/10p joint welded at 1200 rpm and 85 mm/min [41].

shoulder diameters (18, 20, and 22 mm) and threaded cylinder pin were used as FSW tool. They reported that the tensile strength of the weld joints varied from 124 MPa to 172 MPa depending on the tool type and process parameters. A 20 mm shoulder diameter is preferable for obtaining the maximum ultimate tensile strength (UTS). More recently, Kumar et al. [48] investigated the tensile strength of 5 mm rolled Al–4.5%Cu/TiC/10. In order to reveal the effect of three shoulder surface geometries on mechanical properties, full flat surface, 1 mm flat surface, and 2 mm flat surface shoulder with a 7° concave angle were used in FSW. Among the three surface shoulders, the second shoulder configuration resulted in the highest tensile strength. They concluded that the higher heat input as a result of higher contact area between the second shoulder surface and the workpiece led to sufficient mixing in the stirring zone, as compared with the other two tool profiles.

6.2.2. Effect of welding parameters

In FSW process, the welding parameters including tool rotation speed (ω, rpm), traverse speed (V, mm/min) and axial force (F, kN) affect the amount of friction heat generation and mixing process. Therefore, optimum welding parameters must be selected in order to produce the best joint strength. The efficiency of AMC weld joints is generally in the range from 60% to 97% of those of the BM. It is accepted that the UTS of FSW joints of AMCs increases by increasing the rotation speed until a specific limit [37,41,42,47,50,51,53]. The maximum strength was achieved by using a rotation speed ranging from 1000 to 1200 rpm depending on the types of AMC. This leads to the conclusion that there is insufficient heat input in welding joint if the rotation speed is below 1000 rpm, whilst excessive heat input is produced for the weld joint if the rotation speed is more than 1200 rpm. Either case of insufficient or excessive heat input produces inadequate mixing of soft metal. On the contrary, both Yigezu et al. [56] and Kumar et al. [48] reported that the tensile strength decreases linearly when the tool rotational speed increases in FSW rolled Al–12%Si/TiC/10 and rolled Al–4.5%Cu/TiC/10, respectively.

In addition to the tool rotation speed, another important parameter is the traverse speed of the tool along the weld line. A suitable traverse tool stirs the material efficiently from the AS to the RS. Three possible behaviours for the effects of the traverse speed on the tensile strength of AMC joints are discussed below.

Firstly, a unsteady behaviour of the traverse speed on the tensile strength for different types of AMC has been noted. For example, researches [41,47,50] on AA6061 composite aluminium as base matrices showed that the relation between the UTS and the traverse speed is

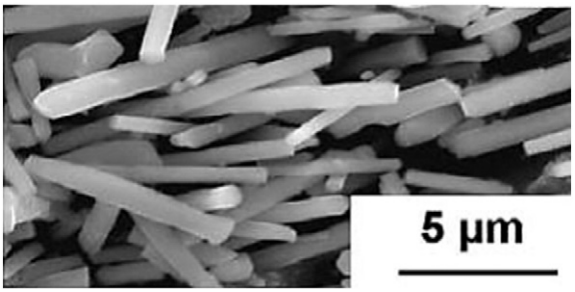

Fig. 13. Reorientation of reinforcement in FSW AA2124/SiC/20w [28].

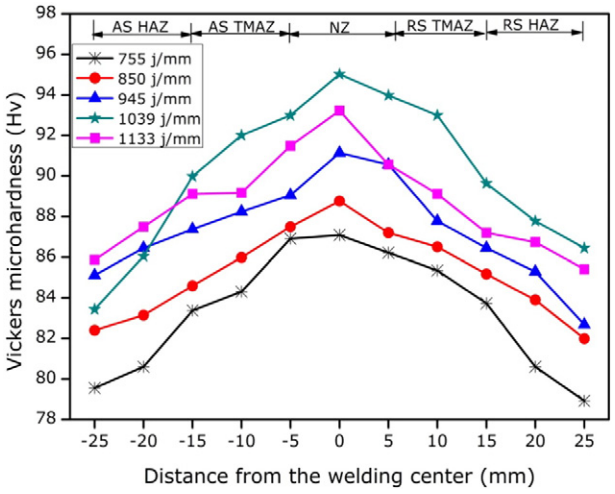

Fig. 14. Microhardness profile across the weld region of AA6061/SiC/10p at different heat inputs following FSW [42].

not directly proportional. As traverse speed increases the tensile strength increases and reaches a maximum value before it decreases. They assert that the amount of heat input due to friction action between the tool and BM is mainly affected by tool rotation speed. On the other hand, the cooling rate is determined by the traverse speed. Therefore, at lower traverse speed an increase in frictional heat generation and slow cooling rate is accompanied by coarse grains (grain growth). Tunnel defects may occur due to excessive stirring resulting from slow traverse speed. In contrast, at higher traverse speeds insufficient heat input is generated into the joint, which leads to inadequate stirring action of softened material from the AS to the RS also causing tunnel defects. Therefore, reduced tensile strength can be resulted from both low and high traverse speeds.

Secondly, a linear behaviour of traverse speed on the tensile strength for AA2009/SiC/17p was reported by Wang et al. [49]. The maximum joint efficiency was achieved to reach 97% of the BM at a higher traverse speed of 800 mm/min. They pointed out that at lower traverse speed failure of the joint happened in the HAZ which was characterised by lowered hardness due to dissolution and precipitates growth. This led to the reduction in tensile strength. On the other hand, as the traverse speed was increased the clusters were partially dissolved in the matrix in the HAZ owing to high cooling rate. Thus an increase in joint efficiency was achieved as a result of the increase of HAZ hardness and shift in fracture location from HAZ to NZ.

Thirdly, as reported by other researchers [48,53,56], the increase of the traverse speed slightly decreases the tensile strength of the joint (inversely proportional) for AMCs AA2124/SiC/25p, Al–4.5%Cu/TiC/10, and

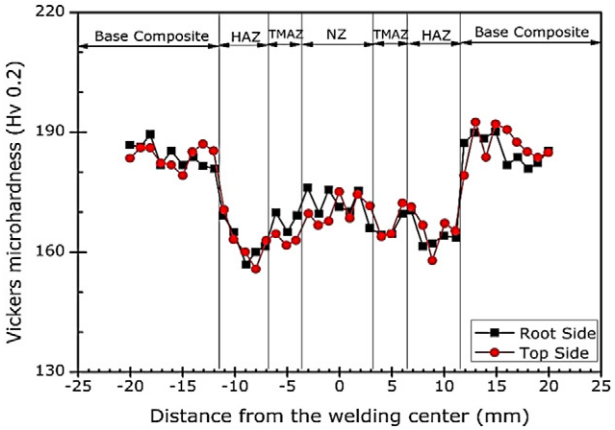

Fig. 15. Microhardness profile across the weld region of AA2124/SiC/25p following FSW [36].

Table 1
Welding variables and tensile properties of AMC joints welded by FSW.

Base metals	Base metal condition	Plate thickness (mm)	Rotation speed (rpm)	Traverse speed (mm/min)	Axial force (kN)	Pin shape	UTS (MPa)	Yield stress (MPa)	EL (%)	Joint efficiency (%)
AA6061/ZrB_2/10 [50]	Cast	6	1155	48.8	5.9	Square	243	–	–	95.8
AA6061/B_4C/12 [51]	Cast	6	997	78	9.3	Square	208	–	–	96.83
AA6061/B_4C/12 [30]	Cast	6	1000	80	10	Square	201	–	2.5	93.4
AA6061/AlNp [52]	Cast	6	1200	55	5	Square	225	–	0.77	93.42
AA 7005/Al_2O_3/10p [34]	Extruded-T6	7	800	56	–	–	260	245	0.58	83.87
AA 6061/Al_2O_3/20p [34]	Extruded-T6	7	800	56	–	–	329	280	1.3	86.80
AA 6061/Al_2O_3/20p [39]	Extruded-T6	7	700	300	–	–	251	234	–	70
AA 6061/Al_2O_3/22p [45]	Cast	4	880	260	–	Cylinder smooth	227	–	–	99
AA 6061/SiC/10p [42]	Cast	6	1100	45	6	Cylinder thread	206	126	6.5	74
AA 6061/SiC/10p [47]	Cast	6	1370	88.9	9.6	Cylinder thread	265	–	–	92.3
AA 2124/SiC/25p [53]	Forged T4	3	1120	40	–	Cylinder thread	366	–	–	81
AA 2124/SiC/25p [40]	Forged-T6	15	550	75	8.5	Conical thread	642	478.8	2.9	86.5
Al/Mg_2Si/15p [37]	Cast	6	1120	125	–	Cylinder thread	110	–	–	95
AA 2009/SiC/15p [32]	Extruded-T4	8	600	50	–	Cylinder thread	450	320	3	95
AA2009/SiC/17p [29]	Rolled-T351	3	1000	50	–	Cylinder	443	274	4.7	76
AA 2009/SiC/15p [33]	Rolled-T4	6	800	100	–	Conical	441	306	5.4	82
AA 2009/SiC/17p [49]	Extruded-T4	3	1000	800	–	Conical thread	501	341	3.5	97
AA 6063/B_4C [38]	Extruded	4.5	1500	600	–	Conical	176	125	2.5	62
Al–4.5%Cu/TiC/10p [48]	Rolled	5	500	20	6	Cylinder thread	173	–	2.83	89

EL: elongation; joint efficiency: the ratio of the tensile strength of joint to the tensile strength of base metal; UTS: tensile strength.

Al–12%Si/TiC/10, respectively. The best welding speeds are 40 mm/min for AA2124 and 20 mm/min for the other two AMCs. However, they mentioned that the influence of traverse speed on UTS is less obvious than the tool rotation speed and tool design.

Applied axial force is another important parameter in FSW. The heat generated by friction between the BM and tool depends on the friction coefficient which is specified by the applied force. Higher heat input is generated by a larger amount of applied force which causes sufficient flow. Defect free joint can be achieved if a sufficient axial force which is higher than the flow stress of the BM is applied. Thus higher tensile strength can be obtained when an adequate force is selected. In spite of the importance of the applied force on the amount of heat generation and the retention of the plasticized metal, few researchers have taken into account the effect of this parameter as one of the key welding variables on tensile strength.

Dinaharan and Murugan [50] reported that the maximum tensile strength of joint was obtained at 6 kN axial force when joining in-situ composite AA6061/ZrB_2. Further increment in hydrostatic pressure leads to a reduction in the tensile strength. The appearance of microvoids in the joint at lower force and excessive flash at larger force causes a reduction in the cross section of the joint and hence leads to a reduction in tensile strength of joint. Similarly, Murugan and Kumar [41] indicated that for the FSW joints of AA6061/AlNp tunnel defects appeared in the cross section of joint due to the lack of heat generation when using lower axial forces. Therefore, a reduction in tensile strength happened when the applied force was lower than 5 kN. On the other hand, if the applied force was more than 5 kN it led to thinning of the NZ and formation of worm hole, and therefore reduced the joint efficiency. A similar finding was reported by Kalaiselvan and Murugan [51] in FSW joints of AA6061/B_4C with a different optimum axial force at 10 kN in their study.

In conclusion, welding parameters including tool rotation speed, traverse speed, and axial force affect significantly the UTS of AMC joints. Rotation speed has the greatest effect on joint efficiency, whilst traverse speed and axial force affect the tensile strength of AMC joints to a varying degree [53]. There is no general trend that can be related to welding parameters for all types of AMCs. Therefore, each material needs its own study to achieve its maximum tensile strength for the FSW joint.

6.2.3. Effect of other factors

There are other factors such as the formation of intermetallic compound, PWHT, and strain rate which also affect the tensile strength of the FSW AMC joints. The formation of intermetallic compounds at the ceramic matrix interface lowers the inner bonding between the reinforcement and matrix. Feng et al. [32] studied the feasibility of joining AA2009/SiC/15p by FSW under annealed condition and followed by PWHT to T4 condition for further strengthening. The tensile strength of the joint was increased by 82% and 95% from the BM in the longitudinal and transverse directions, respectively. 100% joint efficiency in T4 condition cannot be achieved due to the formation of secondary phase (Cu_2FeAl_7) in the NZ as a result of interaction between the tool worn material and the BM. In contrast, Wang et al. [57] succeeded in preventing formation of Cu_2FeAl_7 phase by using ultra hard tool material in FSW AA2009/SiC/15p. The strength of FSW joint was increased from 321 MPa to 521 MPa after PWHT to T4 condition, which is almost the same as the strength of BM at 543 MPa. Recently, Ni et al. [58] studied the effect of strain rate on strain hardening and tensile properties of FSW AA2009/SiC/17p joints. Because of little difference in hardening capacity of both the BM and the joint, slight reduction in tensile strength occurred when the strain rate increased and the fracture of most specimens happened in the HAZ of the RS.

6.3. Fatigue strength of AMC joints

Although many applications of AMC joints by FSW are designed to subject to dynamic loading conditions, there were few studies related to the fatigue properties of AMC joints. Ceshini et al. [35] studied the effect of strain amplitude on low cycle fatigue strength of AA6061/Al_2O_3/20p FSW joints. The fatigue life of FSW joints is lower than the BM under all conditions. This is attributed to the factors such as the modification of welded surface, joint microstructure, and higher amount of plastic strain induced by FSW. The roughness of surface affects significantly the fatigue life when the strain amplitude decreases. Also the isotropic hardening value is higher under low strain amplitudes. At high strain amplitudes, the hysteresis loop area does not change. Moreover more plastic strain happened in FSW joints than in the BM in low cycle fatigue due to progressive hardening as shown in Fig. 16.

It is well known that the behaviour of fatigue is more sensitive to the homogeneity of microstructure than the behaviour of tensile. In an investigation on high cycle fatigue of FSW joint AA7005/Al_2O_3/10p and AA6061/Al_2O_3/20p [59,60], it was reported that the FSW joint of the former material exhibited higher fracture toughness and lower fatigue crack growth, whilst the behaviour of the latter was opposite. Depending on the microstructure it was argued that the volume fraction of reinforcement in AA6061/Al_2O_3/20p was double of that in the AA7005/Al_2O_3/10p. More refined particles formed in the AA6061 matrix after

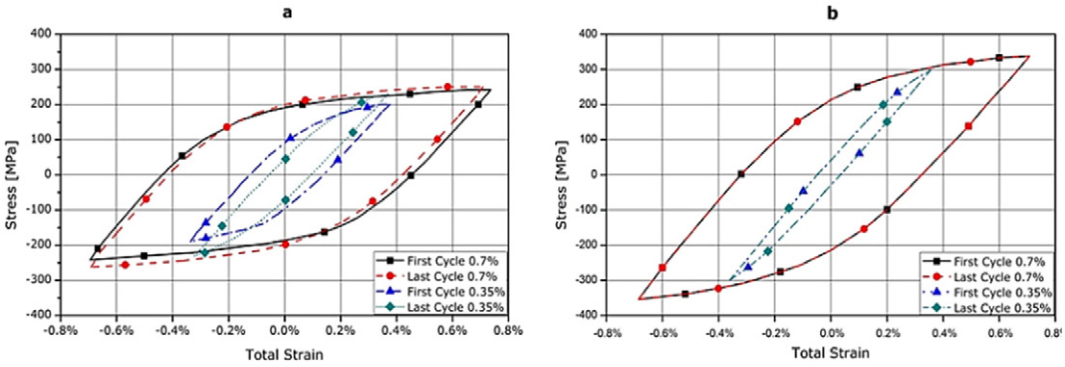

Fig. 16. Hysteresis loops at different strain amplitudes for the FSW (a) and the base metal (b) AA6061/Al_2O_3/20p [35].

FSW led to increased number of stress raisers, embrittlement, and a reduction in the fracture toughness. Therefore, the fracture toughness of AA7005/Al_2O_3/10p joint is higher than the BM by 10–20%, whilst in the case of AA6061/Al_2O_3/20p it is lower than the BM by 25%. However, the crack propagation rate of un-welded AA7005 composite series is higher than AA6061 composite series. Furthermore, Minak et al. [45] reported that the fracture location in the fatigue test shifted from the NZ to the BM as shown in Fig. 17 in AA6061/Al_2O_3/22p FSW joint, as a result of complete penetration.

Furthermore, residual stresses are also induced into FSW joint due to severe plastic deformation of workpiece through the joining process. Ni et al. [61] studied the effect of residual stress on the behaviour of high cycle fatigue of AA2009/SiC/17p FSW joint. X-ray diffraction test showed that the maximum tensile residual stress of 54 MPa was induced along the centreline of the weld joint, whilst residual stresses were in compression being about 70 MPa and 60 MPa in the AS and the RS, respectively. At lower stress amplitudes below 150 MPa, the FSW fatigue samples fractured in the weld zone and gave nearly the same fatigue limit as the BM due to the interaction between the residual stresses and the applied load. But at higher stress amplitude, the fatigue life of FSW joints was lower than that of the BM. Meanwhile, the fracture tended to occur randomly in either the AS or RS of the HAZ.

Finally, for critical engineering applications of AMCs, it is much more important to evaluate the fatigue properties of FSW joints in more depth. For FSW AMC joints, the fatigue strength and fatigue crack growth are affected by several factors such as surface roughness, microstructure homogenization, reinforcement volume fraction, and residual stresses in the weld zone. Also the appearance of the reinforcement on aluminium matrices can play a role in stress concentration. Therefore, there is a need for more effort to understand low cycle fatigue behaviour of AMC joints by FSW.

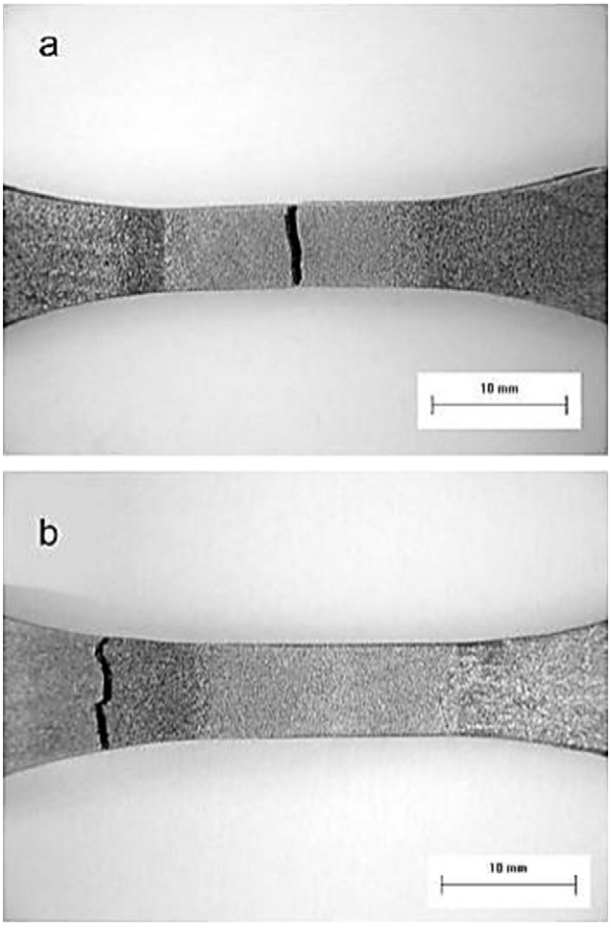

Fig. 17. Fatigue failures in the FSW joint of AA6061/Al_2O_3/22p (a) within the stirred FSW zone, (b) out of the FSW zone [45].

7. Tool wear in FSW of AMCs

Wear of FSW tool is a critical issue particularly for AMC materials, which occurs as a result of friction, rotation, and movement of FSW tool along the base material. According to Rai et al. [7], plastic deformation, abrasion, diffusion, and reaction between the environment and the tool material are the major wear mechanisms that happen in FSW tools. Mishra and Ma [10] reported that FSW of soft metals such as aluminium and magnesium did not exhibit significant wear of the tool. However, tool life issue becomes more significant when hard metals of high melting temperature or MMCs are welded by FSW. This phenomenon is characterised by the deformation and reduction in the pin diameter.

The appearance of hard reinforcement particles in AMCs makes abrasion a dominating factor for tool wear in FSW. Prado et al. [62,63] studied the effect of welding parameters including rotation speed between 500 and 2000 rpm and traverse speed between 1 and 9 mm/s on threaded 1/4–20/01 AISI oil-hardened steel tool wear. Similar joints for AA6061/Al_2O_3/20p and monolithic aluminium AA6061-T6, were used in their studies. They pointed out that no wear was observed in the tool when welding a monolithic aluminium alloy, whilst severe wear started in joining AA6061/Al_2O_3/20p when reaching its maximum value at 1000 rpm then gradually becoming constant after a period of time (self-optimised tool shape). And thus the turbulent flow (vortex flow) of worn tool is less than the unworn tool due to the eroded threads.

Fig. 18 shows the wear features, the rate of tool wear at various weld lengths and the relationship between weld speed and tool wear rate. However, from microstructure evaluation it was found that sound joint could be produced continuously by using tools with self-optimised shapes.

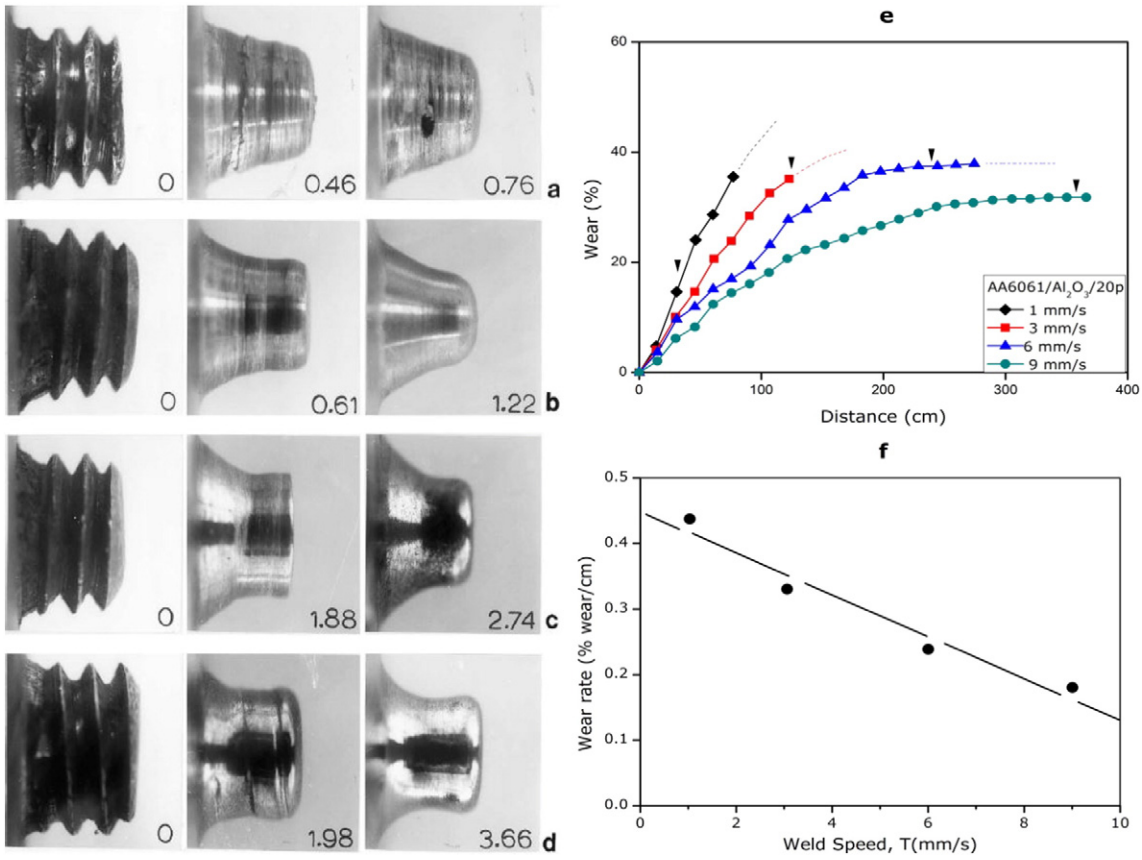

Fig. 18. Wear features of FSW tool pin (a) - (d) at different weld distance (in metres) and constant tool rotation speed of 1000 rpm at different traverse speeds: (a) 1, (b) 3, (c) 6, and (d) 9 mm/s; (e) wear rate versus weld length at different traverse speed and (f) wear rate versus weld speed [63].

The self-optimisation phenomenon of tool shape was confirmed by Shindo et al. [64] and Fernandez and Murr [65] in their experimental investigations by using cast AMC plate, AA359/SiC/20p. An AISI 01 oil-hardened steel threaded 1/4–20 tool was used. Shindo et al. [64] pointed out that there was an inverse relationship between traverse speed and wear rate at constant rotation speed. Fernandez et al. [65] reported that there was a linear relationship between the wear rate and the tool rotation speed. However, as a result of filling threads by base materials, the initial wear of the tool can be delayed by the reduction of rotation speed and the increase in traverse speed and after a period of time the wear rate becomes constant as shown in Fig. 19. They concluded that the self-optimised tool shape was evolved as a result of complex solid-state flow of the BM during FSW. Moreover, they indicated that homogeneous structure could be achieved with a worn pin.

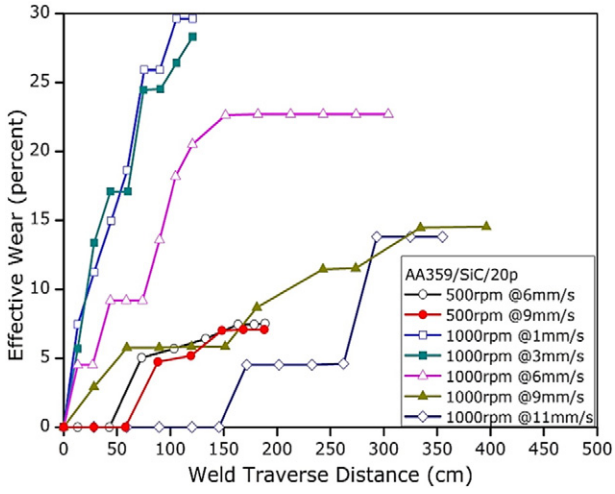

Fig. 19. Pin tool wear as a percent of initial tool shape projections versus weld traverse distance for different tool rotation and traverse speeds [65].

Further improvement of tool life cannot always be achieved by changing the type of steels. For example, Cioffi et al. [40] used MP159 and H13 as tool material for threaded pin and shoulder, respectively. At a rotation speed of 800 rpm, severe wear of the pin happened in welding 15 mm thick AA2124/SiC/25p plates. Chen et al. [38] indicated that the reduction of tool wear could be achieved if tool design was changed. An AISI 4340 unthreaded conical tool was used for joining AA6063/B_4C with limited wear rate. It is clear that significant wear can occur as steels are used in specific design as FSW tool. Moreover, the formation of intermetallic compound is produced as results of interaction between the worn tool material and the BM. Feng et al. [32] showed that the interaction between Fe from worn tool and AA2009/SiC/15p resulted in the formation of Cu_2FeAl_7. The appearance of this compound in the weld zone proves to be detrimental to the joint efficiency, i.e. a reduction of the strength of joint and change of failure modes from ductile to brittle.

Harder materials can be used as tool material rather than steels to reduce wear rate. Ni et al. [29] used cermit tool to weld AA2009/SiC/17p. The tool was not visibly worn at 50 mm/min traverse speed and 1000 rpm rotation speed. In the same manner, Wang et al. [57] reported that the formation of intermetallic compound (Cu_2FeAl_7) during welding AA2009/SiC/15p was eliminated as a result of improved wear resistance of tool by using an ultra-hard material without giving detailed specifications of the tool material. Recently Prater et al. [66] compared wear resistance among different types of tool materials including 01 steel, Wc-Co micron, Wc-Co submicron, and Wc-Co coated by diamond to join AA359/SiC/20p-T6 and AA359/SiC/30p-T6. They observed

that harder material can be used to reduce the wear of tool by 60–80%. However, the toughness of the tool is another problem as it may cause tool fracture in FSW.

Alternatively, surface coating may be used to reduce the occurrence of abrasive wear in the FSW tool. An experimental work was reported by Contorno et al. [67] to modify the wear resistance of the tool surface by generating a tribological layer to join AA359/SiC/20p. They used AISI 1040 cone tool without thread, which has a 1200 Hv substrate coated by a different nano-composite layer of AlSiTiN and AlSiCrN of 5100 and 5200 Hv, respectively. Although they used high hardness coated material, they found that there was no definitive advantage from the coating. On the other hand, Bozkurt et al. [36] reported that the tool wear was eliminated by using high speed steel (HSS) coated by TiAlN. Based on these studies, it seems to be the case that the adhesion force between the substrate and the coated material has a great effect on tool wear rate.

In conclusion, severe wear of FSW tool occurs especially in the pin when steels are used as tool materials for joining AMCs. Tool wear resistance can be improved by changing the design and the material of the pin. Also suitable coating material compatible with the substrate tool material can improve wear resistance. However, there is no work reported on the improvement of wear resistance by using surface heat treatment technique. Therefore more effort in this field is needed for increased tool life and reduced formation of intermetallic compound which has a detrimental effect on joint efficiency.

8. Conclusions and future challenges

This review aims to outline the current state-of-the-art of joining AMCs by FSW with a number of specific issues discussed including the FSW process, the application of MMCs, weldability of aluminium and AMC materials, macro and microstructure, mechanical properties of FSW joint, and tool wear. FSW, as a solid state welding process, is considered to be potentially a viable route for joining AMC materials. Its potential benefits in cost reduction, joint efficiency improvement, and high production accuracy make it even more attractive for the non-weldable series AA2xxx, AA6xxx and AA7xxx. However, the maturity of using this joining process to weld AMCs is still at an early stage in research and has not yet been fully implemented in industry.

The mechanical properties of AMCs joined by FSW are largely dependent on the combined effect of both the composition of AMCs and the FSW processing conditions. Therefore, the mechanical performance of FSW joints should be evaluated accordingly. Early researches showed that FSW is a potential welding process to achieve defect free joints of AMCs. There is a clear need for more efforts to understand the effect of FSW on these materials in adequate depth to meet design and production requirements. For instance, there is a need for systematic studies which take into account the effects of reinforcement percentage and types of reinforcement on joint efficiency. More work is needed to understand the performance of FSW joint of such as AA2124 and AA6092 as base matrices for AMCs with different reinforcement percentages. Also there is a need for joining AMCs to other materials rather than monolithic aluminium alloys such as magnesium alloys, a new candidate material for aerospace application.

Furthermore, welding parameters such as tool rotation speed, traverse speed, and axial force have a significant effect on the amount of heat generation and strength of FSW joints. Macrostructural evaluation showed the formation of tunnel defects due to inappropriate flow of plasticized metal. Microstructural evaluation of FSW joints clearly shows the formation of new fine grains and refinement of reinforcement particles in the weld zone with different amount of heat input by controlling the welding parameters. However, there is no general trend between welding parameters and mechanical properties for different types of AMCs. Further work needs to be carried out to define the welding window of each composite metal for optimised mechanical properties. Also there is very limited data on fatigue strength and fracture toughness of friction stir welded AMCs. More effort is needed to study these properties in more depth to establish the full potential of FSW joints of AMCs.

Finally, the wear of FSW tools, especially of the pin, is up to this time a main issue when joining AMCs and a major hindrance for the application of FSW process in industry. Using new tool designs which have frustum shapes (self-optimised shape), surface coating of pin by appropriate material compatible with the substrate, and surface heat treatment techniques could be viable solutions to improve both the tool life and joint efficiency.

Acknowledgements

The first author gratefully acknowledges the support provided by the Iraqi Ministry of Higher Education and Scientific Research (IMHESR) for funding this work through scholarship no. 5032. This work was also supported by the Engineering and Physical Science Research Council of UK (EP/L02084X/1), International Research Staff Exchange Scheme (IRSES, MatProFuture project, 318,968) within the 7th European Community Framework Programme (FP7).

References

[1] G. Çam, M. Koçak, Progress in joining of advanced materials, Int. Mater. Rev. 43 (1) (1998) 1–44.
[2] A.M. Hassan, M. Almomani, T. Qasim, A. Ghaithan, Effect of processing parameters on friction stir welded aluminum matrix composites wear behavior, Mater. Manuf. Process. 27 (12) (2012) 1419–1423.
[3] K. Suryanarayanan, R. Praveen, S. Raghuraman, Silicon carbide reinforced aluminium metal matrix composites for aerospace applications: a literature review, Int. J. Innov. Res. Sci. Eng. Technol. 2 (11) (2013).
[4] M.B.D. Ellis, Joining of aluminium based metal matrix composites, Int. Mater. Rev. 41 (2) (1996) 41–58.
[5] R.Y. Huang, S.C. Chen, J.C. Huang, Electron and laser beam welding of high strain rate superplastic Al-6061/SiC composites, Metall. Mater. Trans. A Phys. Metall. Mater. Sci. 32 (10) (2001) 2575–2584.
[6] W.M. Thomas, D.G. Staines, I.M. Norris, R. de Frias, Friction stir welding tools and developments, Weld. World 47 (2003) 10–17.
[7] R. Rai, A. De, H.K.D.H. Bhadeshia, T. DebRoy, Review: friction stir welding tools, Sci. Technol. Weld. Join. 16 (4) (2011) 325–342.
[8] Y.N. Zhang, X. Cao, S. Larose, P. Wanjara, Review of tools for friction stir welding and processing, Can. Metall. Q. 51 (3) (2012) 250–261.
[9] P.L. Threadgill, A.J. Leonard, H.R. Shercliff, P.J. Withers, Friction stir welding of aluminium alloys, Int. Mater. Rev. 54 (2) (2009) 49–93.
[10] R.S. Mishra, Z.Y. Ma, Friction stir welding and processing, Mater. Sci. Eng. R Rep. 50 (1–2) (2005) 1–78.
[11] C.C. Tutum, J.H. Hattel, Numerical optimisation of friction stir welding: review of future challenges, Sci. Technol. Weld. Join. 16 (4) (2011) 318–324.
[12] G. Cam, Friction stir welded structural materials: beyond Al-alloys, Int. Mater. Rev. 56 (1) (2011) 1–47.
[13] W. Thomas, E. Nicholas, J. Needham, M. Murch, P. Temple-Smith, and C. Dawes, Friction Stir Butt Welding, International Patent No. PCT/GB92/02203, GB Patent No. 9125978.8, 1991, U.S. Patent No. 5,460,317, 1995. 1991.
[14] J.F. Lancaster, Metallurgy of Welding, Sixth ed. Abington Publishing, Cambridge/England, 1999.
[15] P. Threadgill, A. Leonard, H. Shercliff, P. Withers, Friction stir welding of aluminium alloys, Int. Mater. Rev. 54 (2) (2009) 49–93.
[16] W.J. Arbegast, Friction stir welding after a decade of development — it's not just welding anymore, Weld. J. 85 (3) (2006).
[17] Metal Matrix Composites (MMC) Market for Ground Transportation, Electronics/Thermal Management, Aerospace and Other End-Users — Global Industry Analysis, Size, Share, Growth, Trends and Forecast, 2013–2019, https://www.linkedin.com/pulse/20140605070839-173774513-metal-matrix-composites-market-review2014 (cited 2015; Available from:).
[18] J. Kaczmar, K. Pietrzak, W. Włosiński, The production and application of metal matrix composite materials, J. Mater. Process. Technol. 106 (1) (2000) 58–67.
[19] M. Rosso, Ceramic and metal matrix composites: routes and properties, J. Mater. Process. Technol. 175 (1–3) (2006) 364–375.
[20] J.M. Kunze, C.C. Bampton, Challenges to developing and producing MMCs for space applications, JOM 53 (4) (2001) 22–25.
[21] J. Pakkanen, A. Huetter, C. Poletti, N. Enzinger, C. Sommitsch, J.T. Niu, Friction stir welding of aluminum metal matrix composite containers for electric components, Key Eng. Mater. 611–612 (2014) 1445–1451.
[22] J.J. Rino, D. Chandramohan, K. Sucitharan, An overview on development of aluminium metal matrix composites with hybrid reinforcement, Int. J. Sci. Res. 1 (3) (2012) 2319–7064.
[23] S. Rawal, Metal–matrix composite for space application, JOM 53 (4) (2001) 14–17.
[24] T. Prater, Friction stir welding of metal matrix composites for use in aerospace structures, Acta Astronaut. 93 (2014) 366–373.

[25] G. Mathers, The Welding of Aluminium and Its Alloys, Woodhead Publishing Limited, Cambridge, England, 2002.
[26] Aluminum and Aluminum Alloys, in: J.R. Davis (Ed.) ASM International, 1993.
[27] S. Kou, Welding Metallurgy, Second ed. John Wiley & Sons, New Jersey, 2003.
[28] D. Storjohann, O.M. Barabash, S.S. Babu, S.A. David, P.S. Sklad, E.E. Bloom, Fusion and friction stir welding of aluminum metal–matrix composites, Metall. Mater. Trans. A 36A (2005) 3237–3247.
[29] D.R. Ni, D.L. Chen, D. Wang, B.L. Xiao, Z.Y. Ma, Influence of microstructural evolution on tensile properties of friction stir welded joint of rolled SiCp/AA2009-T351 sheet, Mater. Des. 51 (2013) 199–205.
[30] K. Kalaiselvan, I. Dinaharan, N. Murugan, Characterization of friction stir welded boron carbide particulate reinforced AA6061 aluminum alloy stir cast composite, Mater. Des. 55 (2014) 176–182.
[31] L. Ceschini, I. Boromei, G. Minak, A. Morrri, F. Tarterini, Effect of friction stir welding on microstructure, tensile and fatigue properties of the AA7005/10 vol.% Al_2O_3p composite, Compos. Sci. Technol. 67 (3–4) (2007) 605–615.
[32] A. Feng, B. Xiao, Z. Ma, Effect of microstructural evolution on mechanical properties of friction stir welded AA2009/SiCp composite, Compos. Sci. Technol. 68 (9) (2008) 2141–2148.
[33] D. Wang, B.L. Xiao, Q.Z. Wang, Z.Y. Ma, Evolution of the microstructure and strength in the nugget zone of friction stir welded SiCp/Al–Cu–Mg composite, J. Mater. Sci. Technol. 30 (1) (2014) 54–60.
[34] P. CAVALIERE, E. Cerri, L. Marzoli, J. Dos Santos, Friction stir welding of ceramic particle reinforced aluminium based metal matrix composites, Appl. Compos. Mater. 11 (2004) 247–258.
[35] L. Ceschini, I. Boromei, G. Minak, A. Morri, F. Tarterini, Microstructure, tensile and fatigue properties of AA6061/20 vol.% Al_2O_3p friction stir welded joints, Compos. A: Appl. Sci. Manuf. 38 (4) (2007) 1200–1210.
[36] Y. Bozkurt, H. Uzun, S. Salman, Microstructure and mechanical properties of friction stir welded particulate reinforced AA2124/SiC/25p-T4 composite, J. Compos. Mater. 45 (21) (2011) 2237–2245.
[37] H. Nami, H. Adgi, M. Sharifitabar, H. Shamabadi, Microstructure and mechanical properties of friction stir welded Al/Mg2Si metal matrix cast composite, Mater. Des. 32 (2) (2011) 976–983.
[38] X.G. Chen, M. da Silva, P. Gougeon, L. St-Georges, Microstructure and mechanical properties of friction stir welded AA6063–B4C metal matrix composites, Mater. Sci. Eng. A 518 (1–2) (2009) 174–184.
[39] L.M. Marzoli, A.V. Strombeck, J.F. Dos Santos, C. Gambaro, L.M. Volpone, Friction stir welding of an AA6061/Al_2O_3/20p reinforced alloy, Compos. Sci. Technol. 66 (2) (2006) 363–371.
[40] F. Cioffi, R. Fernández, D. Gesto, P. Rey, D. Verdera, G. González-Doncel, Friction stir welding of thick plates of aluminum alloy matrix composite with a high volume fraction of ceramic reinforcement, Compos. A: Appl. Sci. Manuf. 54 (2013) 117–123.
[41] N. Murugan, B. Ashok Kumar, Prediction of tensile strength of friction stir welded stir cast AA6061-T6/AlNp composite, Mater. Des. 51 (2013) 998–1007.
[42] P. Periyasamy, B. Mohan, V. Balasubramanian, Effect of heat input on mechanical and metallurgical properties of friction stir welded AA6061-10% SiCp MMCs, J. Mater. Eng. Perform. 21 (11) (2012) 2417–2428.
[43] R.D. Fu, R.C. Sun, F.C. Zhang, H.J. Liu, Improvement of formation quality for friction stir welded joints, Weld. J. 91 (2012) 169-s–173-s.
[44] B.L. Xiao, D. Wang, J. Bi, Z. Zhang, Z.Y. Ma, Friction stir welding of SiCp/Al composite and 2024 Al alloy, Mater. Sci. Forum 638–642 (2010) 1500–1505.
[45] G. Minak, L. Ceschini, I. Boromei, M. Ponte, Fatigue properties of friction stir welded particulate reinforced aluminium matrix composites, Int. J. Fatigue 32 (1) (2010) 218–226.
[46] I. Dinaharan, N. Murugan, Effect of friction stir welding on microstructure, mechanical and wear properties of AA6061/ZrB2 in situ cast composites, Mater. Sci. Eng. A 543 (2012) 257–266.
[47] P. Periyasamy, B. Mohan, V. Balasubramanian, S. Rajakumar, S. Venugopal, Multi-objective optimization of friction stir welding parameters using desirability approach to join Al/SiCp metal matrix composites, Trans. Nonferrous Metals Soc. China 23 (4) (2013) 942–955.
[48] A. Kumar, M.M. Mahapatra, P.K. Jha, N.R. Mandal, V. Devuri, Influence of tool geometries and process variables on friction stir butt welding of Al–4.5%Cu/TiC in situ metal matrix composites, Mater. Des. 59 (2014) 406–414.
[49] D. Wang, Q.Z. Wang, B.L. Xiao, Z.Y. Ma, Achieving friction stir welded SiCp/Al–Cu–Mg composite joint of nearly equal strength to base material at high welding speed, Mater. Sci. Eng. A 589 (2014) 271–274.
[50] I. Dinaharan, N. Murugan, Optimization of friction stir welding process to maximize tensile strength of AA6061/ZrB2 in-situ composite butt joints, Met. Mater. Int. 18 (1) (2012) 135–142.
[51] K. Kalaiselvan, N. Murugan, Role of friction stir welding parameters on tensile strength of AA6061–B4C composite joints, Trans. Nonferrous Metals Soc. China 23 (3) (2013) 616–624.
[52] B. Ashok Kumar, N. Murugan, Optimization of friction stir welding process parameters to maximize tensile strength of stir cast AA6061-T6/AlNp composite, Mater. Des. 57 (2014) 383–393.
[53] Y. Bozkurt, A. Kentlİ, H. Uzun, S. Salman, Experimental investigation and prediction of mechanical properties of friction stir welded aluminium metal matrix composite plates, Mater. Sci. 18 (4) (2012).
[54] S.J. Vijay, N. Murugan, Influence of tool pin profile on the metallurgical and mechanical properties of friction stir welded Al–10 wt.% TiB2 metal matrix composite, Mater. Des. 31 (7) (2010) 3585–3589.
[55] A.M. Hassan, T. Qasim, A. Ghaithan, Effect of pin profile on friction stir welded aluminum matrix composites, Mater. Manuf. Process. 27 (12) (2012) 1397–1401.
[56] B.S. Yigezu, D. Venkateswarlu, M.M. Mahapatra, P.K. Jha, N.R. Mandal, On friction stir butt welding of Al + 12Si/10 wt%TiC in situ composite, Mater. Des. 54 (2014) 1019–1027.
[57] D. Wang, B.L. Xiao, Q.Z. Wang, Z.Y. Ma, Friction stir welding of SiCp/2009Al composite plate, Mater. Des. 47 (2013) 243–247.
[58] D.R. Ni, D.L. Chen, D. Wang, B.L. Xiao, Z.Y. Ma, Tensile properties and strain-hardening behaviour of friction stir welded SiCp/AA2009 composite joints, Mater. Sci. Eng. A 608 (2014) 1–10.
[59] A. Pirondi, L. Collini, D. Fersini, Fracture and fatigue crack growth behaviour of PMMC friction stir welded butt joints, Eng. Fract. Mech. 75 (15) (2008) 4333–4342.
[60] A. Pirondi, L. Collini, Analysis of crack propagation resistance of Al–Al_2O_3 particulate-reinforced composite friction stir welded butt joints, Int. J. Fatigue 31 (1) (2009) 111–121.
[61] D.R. Ni, D.L. Chen, B.L. Xiao, D. Wang, Z.Y. Ma, Residual stresses and high cycle fatigue properties of friction stir welded SiCp/AA2009 composites, Int. J. Fatigue 55 (2013) 64–73.
[62] R.A. Prado, L.E. Murr, D.J. Shindo, K.F. Soto, Tool wear in the friction-stir welding of aluminum alloy 6061 + 20% Al_2O_3: a preliminary study, Scr. Mater. 45 (2001) 75–80.
[63] R.A. Prado, L.E. Murr, K.F. Soto, J.C. McClure, Self-optimization in tool wear for friction-stir welding of Al 6061 + 20% Al_2O_3 MMC, Mater. Sci. Eng. A 349 (1–2) (2003) 156–165.
[64] D.J. Shindo, A.R. Rivera, L.E. Murr, Shape optimization for tool wear in the friction-stir welding of cast AI359-20% SiC MMC, Mater. Sci. 37 (2002) 4999–5005.
[65] G.J. Fernandez, L.E. Murr, Characterization of tool wear and weld optimization in the friction-stir welding of cast aluminum 359 + 20% SiC metal–matrix composite, Mater. Charact. 52 (1) (2004) 65–75.
[66] T. Prater, A. Strauss, G. Cook, B. Gibson, C. Cox, A comparative evaluation of the wear resistance of various tool materials in friction stir welding of metal matrix composites, J. Mater. Eng. Perform. 22 (6) (2013) 1807–1813.
[67] D. Contorno, M.G. Faga, L. Fratini, L. Settineri, G. Gautier di Confiengo, Wear analysis during friction stir processing of A359 + 20%SiC MMC, Key Eng. Mater. 410–411 (2009) 235–244.